J Vis (2010) 13:107–119
DOI 10.1007/s12650-009-0002-9

REGULAR PAPER

Seiichiro Asano · Syunsuke Ikeda · Toshiharu Kagawa · Chongho Youn

Visualization of behaviors of a propagating flame quenching for hydrogen–air gas mixture

Received: 10 February 2009 / Revised: 31 July 2009 / Accepted: 18 October 2009 / Published online: 12 December 2009

Abstract In this research, a flame arrester consisting of a slit structure was experimentally investigated. Experimental data show adequate maximum experimental safe gap (MESG) value for the flame arrester. The flow rate characteristics of the flame arrester were measured and compared with theoretical results. It was made clear that the flow impedance of convergent flow is 20% less than that of divergent flow. The experimental data and theoretical data show good agreement. The performance test by an EN12874 as 'in-line stable detonation' flame arrester was examined for a hydrogen–air gas mixture. The experimental data show that the gap was 0.2 times the MESG value in bi-directions for the flame arrester. The quenching and extinguishing processes were visualized by high-speed cameras.

Keywords Hydrogen–air flame · Detonation wave · Flame arrester · Quenching element

1 Introduction

The idea of a society run on hydrogen energy has attracted considerable attention in recent years. Hydrogen gas is called clean energy because it does not emit carbon dioxide upon combustion. Therefore, hydrogen gas is expected to be widely used in both households and industries. Hydrogen gas is used mainly in the fields of fuel cell technology, the desulfurization process of crude oil and hydrogen combustion engines in recent years. For this reason, research has focused on the development and establishment of a new social infrastructure suitable for industrial societies. The safe use of hydrogen gas as an energy source in the future is significantly dependent on the conception of convenient and sufficient methods for its production, storage and transmission.

A flammable range of hydrogen gas is from 4.1 to 75 vol% in air at room temperature, approximately 298 K. It is more necessary to pay attention when using hydrogen gas because the flammable range is wider than other flammable gases. Research on detonation of gases has been done by many researchers. It has been revealed that the cellular structure width leads to a transition from a combustion wave to a detonation wave in a pipe (Ohyagi et al. 1988). The cellular width varies with the stoichiometric gaseous mixture of flammable gases such as ethylene, propane and hydrogen with air and the initial pressure in the

S. Asano · S. Ikeda
Department of Civil and Environmental Engineering, Tokyo Institute of Technology,
M1-1, 2-12-1, O-okayama, Meguro-ku, Tokyo 152-8552, Japan

T. Kagawa · C. Youn (✉)
Precision and Intelligence Laboratory, Tokyo Institute of Technology, R2-45, 4259 Nagatuta,
Midori-ku, Yokohama 226-8503, Japan
E-mail: youn.c.aa@m.titech.ac.jp
Tel.: +81-45-9245485
Fax: +81-45-9245486

pipe (Hikita et al. 1979). The maximum power of detonation is theoretically defined as the stoichiometric mixture ratio. Based on the CJ (Chapman–Jouguet) theory, it is possible to calculate detonation velocity (Lewis et al. 1987). The CJ theory concerns the detonation wave based on the gas dynamic as one-dimensional steady flow. The detonation velocity reaches 1,971 m/s (hydrogen, 27 vol%) at the condition of 295 and 100 kPa by the CJ theory. In the CJ state, a detonation wave propagates to approximately 2,000 m/s theoretically for a hydrogen–air gas mixture (Shepherd 2009).

The flame arrester element is required in a gas pipeline to quench propagating flame. However, minimal flow resistance is also required for the flame arrester element. The quenching and extinguishing process of propagating flame has been studied by both theoretical and experimental analyses, using a dimensionless number, which is the ratio of the cellular structure width to the inside diameter of the pipe (Pantow et al. 1996). Furthermore, a detonation wave was extinguished by a quenching element that had a very narrow gap (Obara et al. 2006). These results showed that the detonation cellular structure width is important to design the quenching element. The smallest width for each gas is as follows: 15 mm (hydrogen, 27 vol% in air), 25 mm (ethylene, 7.0 vol% in air) and 50 mm (propane, 4.0 vol% in air).

There are several national and international standards for the flame arrester (ANSI 1996; US Coastguard 1990; ISO 2008; BS 1990, 2001). These standards are the performance test method for a flame arrester using the maximum experimental safe gap (MESG) value. According to these standards, the MESG values are as follows; 0.29 mm (hydrogen, 27 vol% in air), 0.65 mm (ethylene, 6.5 vol% in air) and 0.92 mm (propane, 4.2 vol% in air). However, there are many types of quenching elements, such as a woven wire gauze, wire mesh, perforated plate, crimped metal ribbon, parallel plate, stacked precision tube and porous material. These have been used in the past or are still being used today (Booklet 1996). The safe gap size for many types of quenching elements must be clarified by their MESG values. To evaluate the MESG values due to propagated flame transmissions, the experiments were conducted for a flame arrester with a quenching element made of crimped metal ribbons (Lietze 2002), and the following criteria were determined: by decreasing the gap length by half, the gap size decreased by a maximum of 0.3 times the MESG value. However, the safe gap size for many types of quenching elements is still insufficient.

On the other hand, the flame structure in explosions has been described in terms of visualization methods, such as high-speed digital imaging (Hargrave et al. 2001), shadowgraph techniques (Matsumoto et al. 2003) and high-speed framing (Kersten et al. 2004). However, this study visualized the behaviors of propagating flame without the flame arrester. Therefore, it is necessary to visualize the behaviors of a propagating flame with the flame arrester in the pipe.

In this research, a flame arrester, consisting of an adequate quenching element called a slit structure, was experimentally investigated. The flow rate characteristics of this flame arrester were measured and compared with theoretical results. The performance test by an EN12874 (CEN 2001) as ‘in-line stable detonation’ flame arrester was examined for a hydrogen–air gas mixture. The MESG values were investigated by varying the gap size and slit length. A total of 18 cases were carried out in the experiment. In addition, the detonation wave was observed by a pressure sensor and the propagating flame was visualized by high-speed cameras.

2 IEC general test performance

2.1 Classification of requirements for flame arresters

The flame arresters are set up in a gas pipeline to quench propagating flame. The flame arresters should be designed and located to be able to minimize resistance flow rates as well as to quench propagating flame transmission. The performance test of the flame arrester was defined as the European flame arrester standard (EN12874). The flame arrester classifications for deflagration, stable, and unstable detonations are shown in Table 1. The performance tests are classified into six categories by the locations and the differences in the state of flame. In this study, in-line stable detonation test [application (d) in Table 1] was performed. The state of ‘in-line stable detonation’ means that the flame was propagated along the pipe to the CJ detonation velocity.

2.2 Specification of explosion group

Flammable gases such as methane, propane, ethylene and hydrogen are classified by the EN12874 standard as shown in Table 2. There are three main explosion groups, classified by hazard level: IIA (propane), IIB

Table 1 Flame arrester classification for deflagration, stable and unstable detonation (see in EN12874)

Application		Flame arrester classification
(a)	An confined deflagration into an enclosure or vessel	End-of-line deflagration
(b)	A confined deflagration propagating along a pipe into connecting pipework	In-line deflagration
(c)	A deflagration confined by an enclosure or pipework (length to diameter ratio <5) to the out-side atmosphere or into connecting apparatus	Pre-volume deflagration
(d)	A stable detonation propagating along a pipe into connecting pipework	In-line stable detonation
(e)	An unstable detonation propagating along a pipe into connecting pipework	In-line unstable detonation
(f)	A stable detonation into an enclosure or vessel	End-of-line stable detonation

Table 2 Specification of gas/air-mixtures for deflagration and detonation wave (see in EN12874)

	Range of application		Requirements for test mixture	
	Explosion group	MESG of gas/air mixture (mm)	Gas type	Gas in air by volume (%)
(a)	IIA	0.94 ± 0.02	Propane	4.2 ± 0.2
(b)	IIB1	0.83 ± 0.02	Ethylene	5.0 ± 0.1
(c)	IIB2	0.73 ± 0.02		5.5 ± 0.1
(d)	IIB3	0.67 ± 0.02		6.5 ± 0.5
(e)	IIB	0.48 ± 0.02	Hydrogen	45.0 ± 0.5
(f)	IIC	0.31 ± 0.02	Hydrogen	28.5 ± 2.0

(ethylene and hydrogen) and IIC (hydrogen). The group IIB is divided into four sub-groups of IIB1, IIB2, IIB3 and IIB according to mixture ratio. When the hazard level is increased, the MESG value becomes smaller. The MESG stands for the maximum experimental safe gap of these flammable gases mixed with air. In this study, the most hazardous explosion group IIC (hydrogen gas in Table 2) was used.

2.3 Limits of performance

The experiment should be performed under conditions of a surrounding temperature between 253 and 333 K, and a pressure between 80 and 110 kPa according to the EN12874 standard. The MESG value can be defined in this range. Therefore, a flammable gas mixture air performance has limits. There are the following limitating conditions on the performance of in-line stable detonation [application (d) in Table 1]:

1. Measured in both flame velocity and detonation pressure by a flame detector and pressure transducer frequency response equal to or greater than 100 kHz.
2. Measured in flame velocity greater than 1,900 m/s for group IIC (hydrogen).
3. Set up an element gap of less than of 0.29 mm in accordance with the MESG value (see in Table 1) for group IIC (hydrogen).
4. Set up the pipe on the non-ignition side that shall have ten times the internal pipe diameter, greater than 3 m.

2.4 Procedure

Experimental apparatus for the detonation velocity and pressure measurement is shown in Fig. 1. It consisted of a ball valve, a flame arrester, an ignition source, pressure transducers, photo transistors, a 16 bit A/D converter and a PC. The experiment was performed with a flame arrester and without it. The diameter of the pipe was 20 mm, and it was the same as the previous research (Lietze 2002). With a flame arrester, ignition side pipe length was 5.2 m, non-ignition side pipe length was 4.7 m and flame arrester length was 0.2 m. The total pipe length was 10.2 m. Without a flame arrester, the 0.2 m flame arrester was replaced by 2 m of pipe length to match the total volume. The total pipe length was 12 m.

The pipe was evacuated to almost 0 kPa, and then continuously evacuated for half an hour to remove the vapor in the pipe. The hydrogen–air gas mixture in the mixing vessel was charged to the pipe, and the pressure of the pipe was increased to 150 kPa. The gas mixture inside the pipe was ignited by an electrically

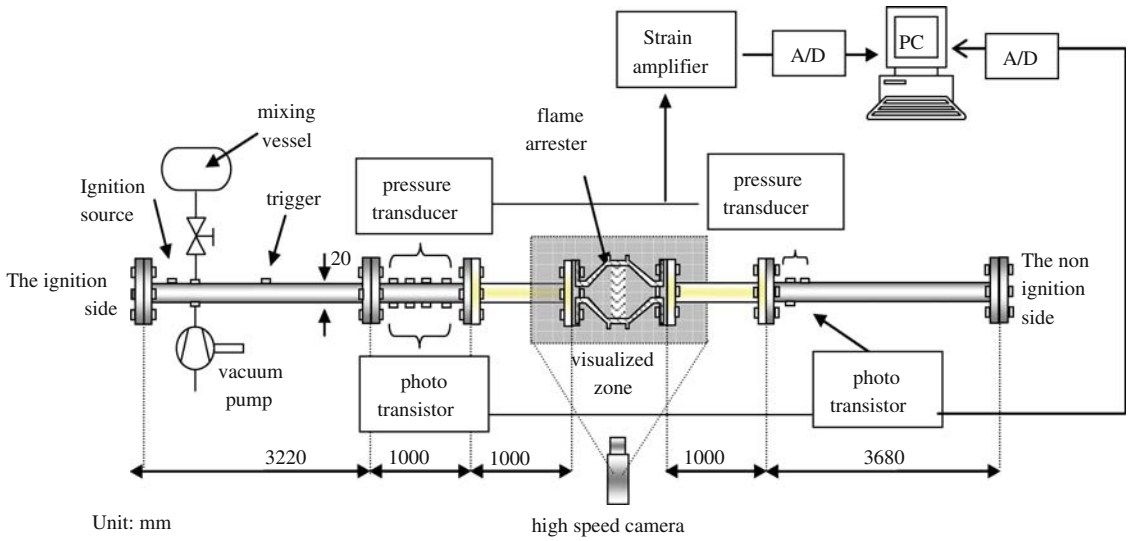

Fig. 1 Experimental apparatus for the detonation velocity and pressure measurement

heated metal wire. The metal wire was located at the end of the ignition side. The detonation wave was observed by a pressure sensor. To visualize a propagating flame, transparent polycarbonate pipes were set up before the flame arrester and after it. And the propagating flame was visualized by high-speed cameras.

2.5 Sensor specification and calibration

The pressure transducer was a PGL-A-20MP-A (Kyowa Electronic Instruments Co. Ltd), which had a 210 kHz natural frequency, and a pressure range of 0–20 MPa. The 6-channel multi-zone control strain amplifier was a 6M92 (NEC Avio Infrared Technologies Co. Ltd). The photo transistor was a TPS601AF (Toshiba Co. Ltd), which had a 500 kHz of natural frequency. The experimental data were recorded by a GR-7500 as an A/D converter (KEYENCE Co. Ltd), which had a 20 MHz sampling rate.

Two high-speed cameras were used to observe the propagating flame. One was a VFC-2000SC (For-A Co. Ltd) with a frame rate of 15,000 Hz in steps of 0.067 ms. It visualized the propagating flame with a flame arrester. Its optical resolution was 512 × 72 pixels with RGB color band. The other was a Phantom V12 (Nobby Tech. Ltd) with a frame rate of 100,000 Hz in steps of 0.01 ms. It visualized the propagating flame without a flame arrester. Its optical resolution was 512 × 96 pixels.

All of the pressure transducers were calibrated with loads of the mechanical press and the oil pressure of the hydraulic chamber. These calibrated pressure data indicated the linearity. All of the photo transistors were calibrated with an LED light source.

3 Flow rate characteristics of flame arrester

3.1 Development of the flame arrester

A flame arrester consists of the housing body and quenching element. The slit structure was developed as a new quenching element. Figure 2 shows a schematic drawing of the newly developed slit structure. The slit structure consists of three elements: a centered hollow plate (disk-a), a cover plate (disk-b) and a pair of spacers. The very narrow spacers are located between disk-a and disk-b and are fixed by bolts. The slit gap size is changed by varying the thickness of the spacers. The slit structure is set up in the housing body as shown in Fig. 3.

The parameters of the slit structure are listed in Table 3. The effect of slit gap size and slit length is investigated. The parameter of slit gap size is 0.06, 0.12 and 0.18 mm and the parameter of slit length is 11, 13 and 15 mm. There are nine types of slit structure.

The effect of flow direction is also examined. A schematic drawing of bi-directional element is shown in Fig. 4. In direction A, the compressed fluid enters from the inner side of disk-a to flow to its outer edge. The

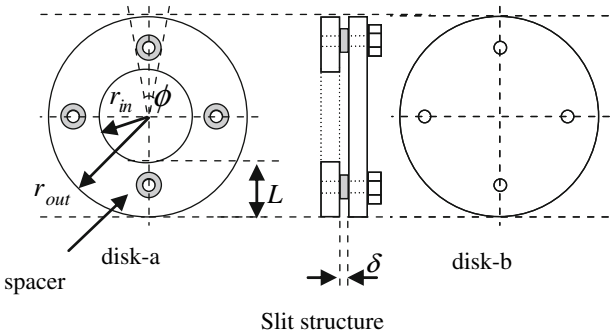

Fig. 2 Schematic drawing of quenching element (slit structure of flame arrester)

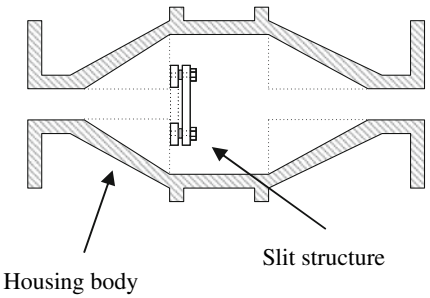

Fig. 3 Schematic drawing of flame arrester

flow channel made by the two disks produces a divergent flow. In contrast, in direction B, the compressed fluid enters from between the outer edge of disk-a and disk-b, and then flows to the inner edge of disk-a. The flow channel made by the two disks produces a convergent flow. Therefore, 18 case experiments are conducted in this study.

3.2 Pressure drop of quenching element

The flow rate characteristics of the slit structure were investigated theoretically under the assumptions that the flow was laminar and passed through the slit under isothermal conditions (Kawashima et al. 2007; Chongho et al. 2008). The relationship between the pressure drop dP and the average flow velocity is given by the following equation.

$$\mathrm{d}P = -\frac{12\mu\bar{u}}{\delta^2}\mathrm{d}r. \tag{1}$$

Considering the continuity equation (2), Eq. 1 yields the following equation (3):

$$(\rho uA)_{r_{\mathrm{in}}} = (\rho uA)_{r_i} r_{\mathrm{in}} < r_i < r_{\mathrm{out}} \tag{2}$$

$$\Delta P = \sqrt{\frac{12\mu G P_a}{\rho\pi\delta^3((\pi - 2\phi)/\pi)}\ln\frac{r_{\mathrm{out}}}{r_{\mathrm{in}}} + P_a^2} + \xi\frac{\rho\overline{u_{\mathrm{in}}}^2}{2} \tag{3}$$

where μ and ρ are the viscosity and density, respectively. δ and ϕ are gap size and the degree of the spacers, respectively. ξ is the inlet coefficient, whose value of 0.2 was chosen to approximately match the experimental results. $\bar{u}_{\mathrm{in}}$ is spatial average flow velocity in the slit inlet. ΔP is the total pressure drop which was

Table 3 Parameters of the slit structure

r_{in} (mm)	r_{out} (mm)	L (mm)	δ (mm)
17, 15, 13	28	11, 13, 15	0.06, 0.12, 0.18

Slit length L is the difference of radii r_{out} and r_{in}; $L = r_{\mathrm{out}} - r_{\mathrm{in}}$

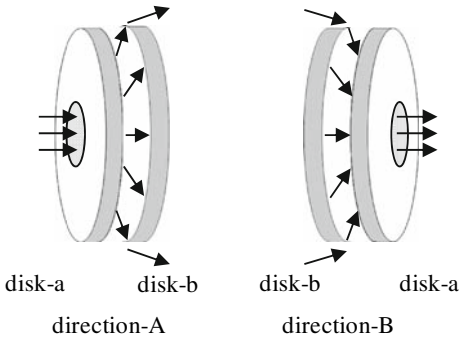

Fig. 4 Schematic drawing of bi-directional flow

given by adding the losses in the slit and the inlet region. In the right side of Eq. 3, the first term stands for the pressure drop by the viscosity. The second term stands for the inlet pressure loss considering the inlet shape of the slit structure.

If the differential pressure was greater than 200 kPa, the flow might have transitioned from laminar to turbulent. The pressure drop of the turbulent flow in the slit structure is given by the following equation (Nakayama et al. 1999).

$$\Delta P = P_a + \lambda \frac{L\rho\overline{u_{in}}^2}{\delta \quad 2} \tag{4}$$

where λ is the friction coefficient. ΔP is the total pressure drop which was given by the dynamic losses associated with the inlet velocity and the addition of atmospheric pressure.

3.3 Flow rate characteristics

The flow characteristics were investigated theoretically and experimentally. The results are shown in Figs. 5, 6, 7. The vertical axes show mass flow rate, and the horizontal axes show supply pressure. The mass flow rate is calculated by Eq. 2. The supply pressure is defined as the sum of ΔP and atmospheric pressure. The characteristics were measured by the ISO 6358 standard with pneumatic system (ISO 1989). In the figures, the plotted data show the experimental results and the dashed and solid lines show the calculation results using Eqs. 3 and 4, respectively. The experimental data were from a total of 18 cases based on three gap sizes, three slit lengths and two directions (directions A and B).

These results show that when the supply pressure was lower than 200 kPa, the plotted data agreed well with the calculation results. However, the fitting curve of Eq. 3 disagreed with the experimental data as the supply pressure increased. In contrast, the calculation results using Eq. 4 showed good agreement across the

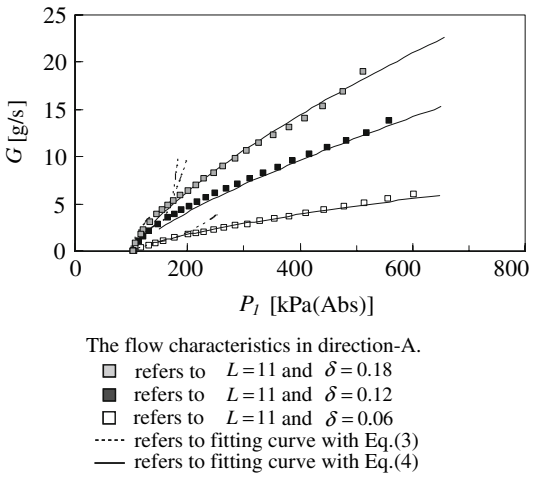

Fig. 5 Variation of three slit gap sizes

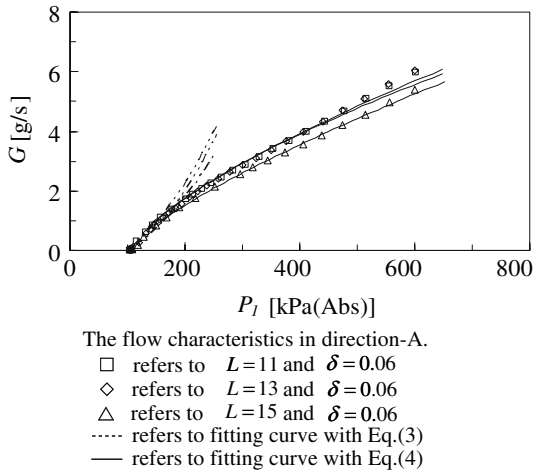

Fig. 6 Variation of three slit lengths

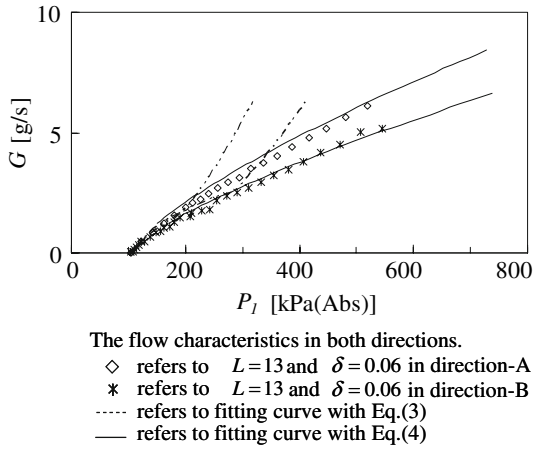

Fig. 7 Variation of two flow directions

whole pressure range. Therefore, the flow characteristics of the slit structures are described on a wide pressure range by fitting with Eq. 4.

3.3.1 Effects of slit gap size

Figure 5 shows that the parameters $\delta = 0.06$, 0.12 and 0.18 mm varied under the constant condition of $L = 11$ mm in direction A. The experimental data agreed well with Eq. 4. When the supply pressure is 400 kPa, the flow rate was 4, 10 and 14 g/s, respectively. This indicates that the gap size of the slit structure affects its flow rate. The flow impedance decreased when the gap size increased. The gap size influenced the other slit length in direction B similarly.

3.3.2 Effects of slit length

Figure 6 shows that the parameters $L = 11$, 13 and 15 mm varied under the constant condition of $\delta = 0.06$ mm in direction A. When the supply pressure was 400 kPa, the flow rate was 4.0, 4.0 and 3.6 g/s, respectively. The flow rates of $L = 11$ and 13 mm were about 8% larger than that of $L = 15$ mm, even if the maximum variation of the slit lengths was approximately 27%. Therefore, the flow impedance slightly decreased when the decrease of slit length is large. The slit length influenced the other gap size in direction B similarly.

3.3.3 Effect of flow direction

Figure 7 shows the bi-directional flow characteristics under the condition of $L = 13$ mm and $\delta = 0.06$ mm. When the supply pressure was 400 kPa, the flow rate was 4.7 and 3.8 g/s in directions A and B, respectively. The flow rate in direction A was approximately 20% greater than that in direction B. The friction coefficient λ was chosen to approximately agree with the experimental results and Eq. 4. The friction coefficient λ was 0.048 and 0.055 for directions A and B, respectively. Therefore, the flow impedance in direction A was 20% smaller than that in direction B. The slit direction influenced the other gap sizes and slit lengths similarly.

4 Quenching characteristics of flame arrester

4.1 Pressure measurement and visualization

4.1.1 Observed pressure and detonation wave velocity

The pressure was measured without a flame arrester. The hydrogen–air gas mixture was charged at 150 kPa. The pipe length was 12 m and both ends of it were closed. The observed pressure from points A to E is shown in Fig. 8. The points A–E refer to 4.0, 4.2, 4.8, 5.0 and 5.4 m in terms of the distance from the ignition source. The pressure rose rapidly to maximum value and gradually decreased.

There were only five pressure sensors in this study, so, the pressure was observed by varying the measurement point. The number of measurement points along the length of the pipe was 20 in total (1.0, 1.2, 1.8, 2.0, 2.4, 4.0, 4.2, 4.8, 5.0, 5.4, 7.0, 7.2, 7.8, 8.0, 8.4, 10.0, 10.2, 10.8, 11.0, 11.4 m). The experiment was conducted 11 times at every 20 points. The maximum, minimum and mean pressures are shown in Fig. 9. The mean pressure around 1 m from ignition source was about 15 MPa; this value was 100 times the initial pressure in the pipe. The mean pressure decayed to about 8.0 MPa from 1 m to the end of pipe.

The velocity of pressure wave was calculated by dividing the observed pressure by the distance between the measurement points. The maximum, minimum and mean velocities are shown in Fig. 10. The range of mean velocities was from 1,783 to 2,146 m/s, and the average of the mean velocities was 1,973 m/s along the pipe across the whole region. The average velocity was almost the same as the CJ detonation velocity, which is defined as 1,971 m/s (hydrogen, 27 vol%). Therefore, the chemical reaction around the ignition source can be considered to have given rise to turbulent combustion, and the detonation wave occurred within 1 m of the ignition source.

The detonations were traveling in excess of the CJ detonation velocity until 1.0 m or less, which was the overdriven detonation region. After the overdriven detonation, the pressure decayed to around 8.0 MPa. Due to backward detonation results in the pressure, it gradually increased in the stable detonation region 10 m from ignition source.

The stable detonation wave was measured in this experiment. Therefore, this experimental apparatus can satisfy the condition of the in-line stable detonation test [application (d) in Table 1].

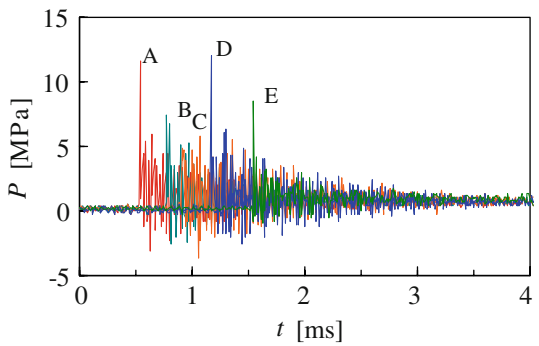

Fig. 8 Pressure response from points A to E

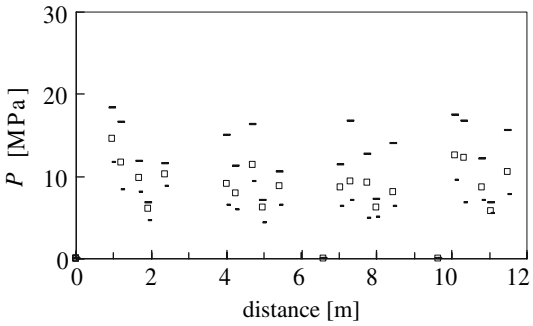

The observed pressure at each measurement point
- refers to maximum pressure of propagation
- refers to mean pressure of propagation
- refers to minimum pressure of propagation

Fig. 9 Pressure at each measurement point (11 experimental results)

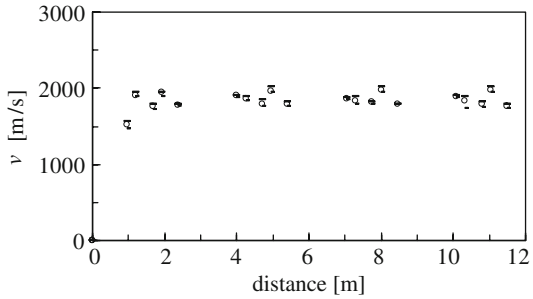

The observed velocity at each measurement point
- refers to maximum velocity of propagation
- refers to mean velocity of propagation
- refers to minimum velocity of propagation

Fig. 10 Detonation wave velocity at each measurement point

4.1.2 Visualization of propagating flame

A propagating flame was visualized at 5.2 m from the ignition source at 0.1 ms intervals, as shown in Fig. 11. The flame arrester was set up at this place. The flame colors were yellow and orange, and it is speculated that some impurities existed in the pipe. The flame propagated from the left hand side to the right hand side.

A flame was propagated in an unburned gas mixture (image a), which existed before the ignition in the pipe. A flame expanded gradually due to a chemical reaction between burned and unburned gas, and then propagated to the non-ignition side (image b, c). The propagating flame reflected at the end of the non-ignition side, and then flame direction changed to the end of ignition side (image d). Moreover, the reflected flame is mixed with burned gas, so the most brightness flame occurs. It was called flame core (image e, f). The flame core propagated to the end of ignition side (image g–l). The flame core reflected at the end of the ignition side and returned again to the end of the non-ignition side (image m). The reflected flame was propagated and weakened progressively to the non-ignition side (image n). Eventually, the flame repeats the reflection until hydrogen–air gas mixture burns out. The duration time of propagating flames is shown in Fig. 12. The duration time was about 20–25 ms.

4.2 Propagating flame quenching

The flame arrester had two different flow impedances. In order to find the quenching characteristics of the bi-directional flow, the flame arrester was located at a distance of 5.2 m from the ignition source. The results of the propagating flame's time duration with $\delta = 0.06$ mm and $L = 13$ mm are shown in Fig. 12. The visualization in both directions A and B is shown in Figs. 13 and 14.

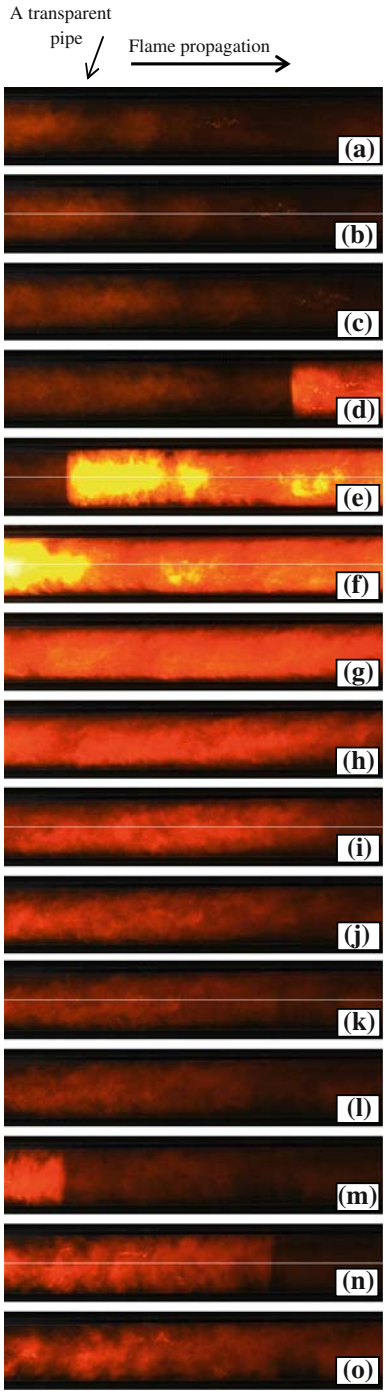

The visible propagation flame in chronological order
Experiments were conducted without the flame arrester

Image (a) refers to the basing point; (b) refers to + 0.1 ms; (c) refers to + 0.2 ms; and at regular interval to (o).
Flames propagated from the left hand side to the right hand side

Fig. 11 Propagating flames along the pipe

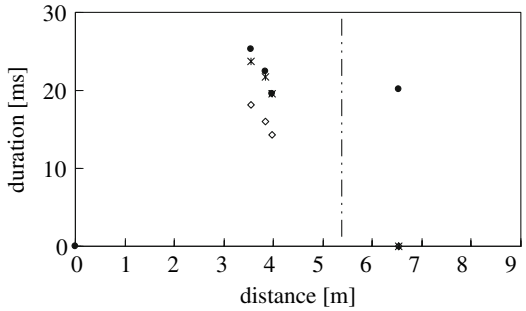

Flame duration along pipe with/without a flame arrester
• refers to without flame arrester
◇ refers to $L = 13$ and $\delta = 0.06$ in direction-A
∗ refers to $L = 13$ and $\delta = 0.06$ in direction-B
--- refers to the position where the flame arrester set upin 5.2 m in length from the ignition source

Fig. 12 Duration of propagating flames along the pipe

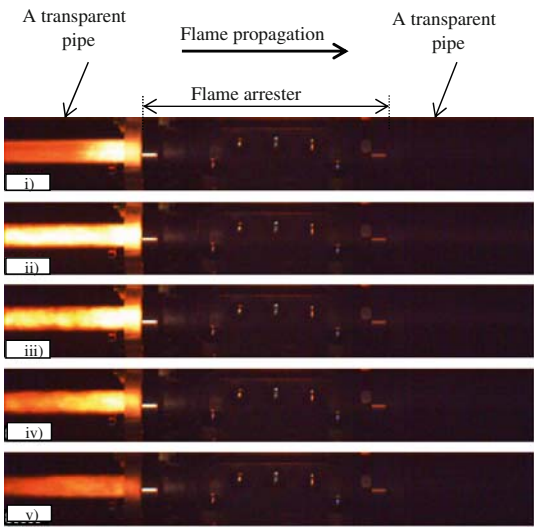

The visible quenching flame in chronological order
Experiments were conducted in direction-A

i) refers to basing point; ii) refers to + 0.67 ms ;
iii) refers to + 1.33 ms ; iv) refers to 2.0 ms;
and v) refers to 2.67 ms.
Flames propagated from the left hand side to the right hand side

Fig. 13 Visualization of propagating flames (direction A)

4.2.1 Quenching characteristics in direction A

The visualization of propagating flames with the flame arrester located in direction A at a distance of 5.2 m from the ignition source at intervals of 0.67 ms is shown in Fig. 13. The unburned gas was supplied through the gaps of the slit structures from the non-ignition side. However, the flame propagation was extinguished and was not transmitted to the non-ignition side. Consequently, the flame core was stagnated inside the quenching element for approximately 20 ms (see Fig. 12).

4.2.2 Quenching characteristics in direction B

The visualization of propagating flames in direction B is shown in Fig. 14. The unburned gas was supplied through the gaps of the slit structures from the non-ignition side. According to the results of the flow

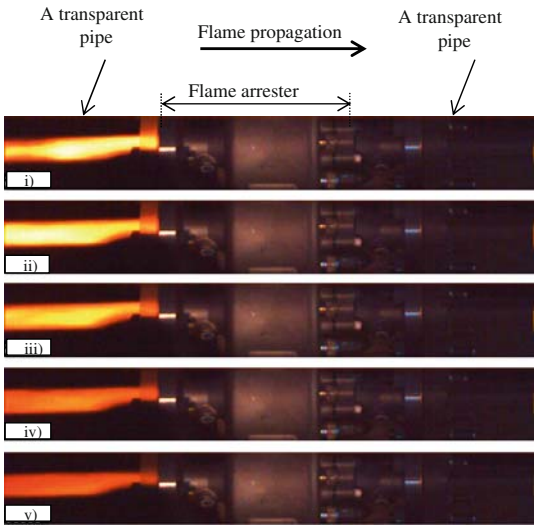

The visible quenching flame in chronological order
Experiments were conducted in direction-B

i) refers to basing point; ii) refers to + 0.67 ms ;
iii) refers to + 1.33 ms ; iv) refers to 2.0 ms;
and v) refers to 2.67 ms.
Flames propagated from the left hand side to
the right hand side

Fig. 14 Visualization of propagating flames (direction B)

characteristics (see Fig. 7), the flow impedance in direction B was 20% greater than that in direction A. Hence, the supply rate from the non-ignition side in direction B was less than that in direction A. As a result, the time duration of propagating flames in direction B was around 25 ms (see Fig. 12). As in direction A, the flame propagation was extinguished and not transmitted to the non-ignition side.

4.2.3 Quenching characteristics for the 18 cases tested

The experiment was conducted, using a slit structure, for three gap sizes, three slit lengths and two directions, totaling 18 cases (see Table 3). Table 4 shows experimental results for the flame quenching or flame transmission in all cases. The gap sizes are listed in three rows and the slit lengths are listed in three columns; directions A and B are listed in each column. The denominator signifies the total number of trials for each case, and the numerator signifies the number of quenchings. When the numerator is equal to zero, it means that the flames were transmitted through the flame arrester.

In the case of $\delta = 0.06$ mm, regardless of slit lengths and directions, the flames were quenched. The gap size was 0.2 times of the MESG value (0.29 mm for hydrogen, 27 vol%). In the case of $\delta = 0.12$ mm, the gap size was 0.4 times the MESG value, and the flames were quenched only in direction B for the all conditions of slit length. However, in the case of $\delta = 0.18$ mm, the gap size was 0.6 times the MESG value and a propagating flame was transmitted for all conditions of slit length.

Table 4 Experimental results for the flame quenching or flame transmission of all cases

	11 mm		13 mm		15 mm	
	Direction A	Direction B	Direction A	Direction B	Direction A	Direction B
0.06 mm	Quenched (11/11)	Quenched (11/11)	Quenched (11/11)	Quenched (11/11)	Quenched (11/11)	Quenched (11/11)
0.12 mm	Transmitted (0/5)	Quenched (11/11)	Transmitted (0/5)	Quenched (11/11)	Transmitted (0/5)	Quenched (11/11)
0.18 mm	Transmitted (0/5)	Transmitted (0/5)	Transmitted (0/5)	Transmitted (0/5)	Transmitted (0/5)	Transmitted (0/5)

Fractions refer to the ratios of flame quenching. Denominators refer to the number of all trials for each case. Numerators refer to the numbers of flames quenched

In summary, the gap size in direction A was greater than or equal to 0.2 times the MESG value and less than 0.4 times. However, the gap size in direction B was greater than or equal to 0.4 times the MESG value and less than 0.6 times.

5 Conclusion

In this research, a flame arrester consisting of a slit structure was developed. In order to determine both the flow rate and quenching characteristics of the flame arrester, an experiment was conducted with a total of 18 cases. The flow rate characteristics of the slit structures were investigated theoretically and experimentally. The experimental data and theoretical data show good agreement. Changing the slit gap size had a greater influence than changing the slit length. It was made clear that the flow impedance of convergent flow is 20% less than that of divergent flow.

The performance test by an EN12874 as 'in-line stable detonation' flame arrester was examined for a hydrogen–air gas mixture; the mixture ratio was 27 vol%. The average of the mean velocities was 1,973 m/s along the pipe across the whole region. The average velocity is almost the same as the CJ detonation velocity. Therefore, it is considered that the detonation wave occurred. The propagating flame was visualized by high-speed cameras. The experimental data show that the gap was 0.2 times the MESG value in bi-directions for the flame arrester. The quenching and extinguishing processes were also visualized by high-speed cameras. So, the slit structures can be applied as the flame arrester. The propagating flame was extinguished by the slit structure with a suitable gap size and slit length.

In a future study, it would be necessary to examine and generalize the effects of the following parameters: fuel, density of the fuel–air mixture and pipe diameter.

Acknowledgments The authors appreciate the advice and support by Kaneko Sangyo Co. Ltd. The authors also appreciate cooperation with For-A Co. Ltd and Nobby Tech. Ltd.

References

ANSI/UL525 (1996) Standard for flame arresters, 6th edn. Underwriter's Laboratory, Inc, USA
BS 7244 (1990) Flame arresters for general use. British Standards Institute, London
BS EN12874 (2001) Flame arresters—performance requirements, test methods and limits for use. The European Standard
Chongho Y, Asano S, Kawashima K, Kagawa T (2008) Flow characteristics of pressure reducing valve with radial slit structure for low noise. J Visualization 11(4):357–364
Flame arresters Booklet, HS (G) 158 (1996) Health and safety Executive
Hargrave GK, Williams TC, Jarvis S (2001) High-speed visualization of flame propagation in explosions. J Visualization 4–4:357–364
Hikita T, Akita K (1979) Introduction to combustion. Corona Publishing, USA, pp 96–115
ISO 6358 (1989) Pneumatic fluid power components using compressible fluids—determination of flow-rate characteristics
ISO 16852 (2008) Flame arresters—performance requirements, test methods and limits for use
Kawashima K, Chongho Y, Kagawa T (2007) Development of a nozzle-flapper type servo valve using a slit structure. Trans ASME J Fluid Eng 129(55):573–578
Kersten C, Forster H (2004) Investigation of deflagrations and detonations in pipes and flame arresters by high-speed framing. J Loss Prevent Process Ind 17:43–50
Lewis B, Elbe VG (1987) Combustion flames and explosions of gases. Academic Press, New York
Lietze D (2002) Crimped metal ribbon flame arrestors for the protection of gas measurement systems. J Loss Prevent Process Ind 15:29–35
Matsumoto S, Nakamura Y, Itoh S (2003) Visualization and numerical analysis of stress waves in blasting process. J Visualization 6(3):235–244
Nakayama Y, Boucher RF (1999) Introduction to fluid mechanics. Butterworth-Heinemann, London
Obara T, Sentanuhady J, Tsukada Y, Ohyagi S (2006) A study on behavior of detonation wave passing through narrow grooves. Trans Jpn Soc Mech Eng B 72(718):1605–1612
Ohyagi S, Ochiai T, Yoshihashi T, Harigaya Y (1988) Relation between cell size, induction zone length and critical initiation energy in oxyhydrogen detonations. Trans Jpn Soc Mech Eng B 54(508):3559–3564
Pantow EG, Fischer M, Kratzel Th (1996) Decoupling and recoupling of detonation waves associated with sudden expansion. Shock Waves 6:131–137
Shepherd JE (2009) Detonation in gases. In: Proceeding of the combustion institute, vol 32, pp 83–89
US Coastguard Standard (1990) Federal Register, 55, Rules and Regulations, p 120